ELSEVIER

Journal of Environmental Management 84 (2007) 347–361

Journal of Environmental Management

www.elsevier.com/locate/jenvman

Capturing fugitive methane emissions from natural gas compressor buildings

R. Litto*, R.E. Hayes, B. Liu

Department of Chemical and Materials Engineering, University of Alberta, Edmonton, Alta., Canada T6G 2G6

Received 28 February 2005; received in revised form 3 April 2006; accepted 7 June 2006
Available online 7 August 2006

Abstract

Fugitive methane emissions account for about 50% of the greenhouse gas (GHG) emissions from the Canadian conventional oil and gas sector. Sources include leaks in natural gas transmission facilities such as pipelines and compressor stations. There are three sources of methane emissions in a compressor station. The first is emissions resulting from incomplete combustion in the engine; the second is leaks in valves, flanges and other equipment in the building; and the third results from instrument venting. Fugitive methane emissions may be in low concentration relative to air, and thus cannot be destroyed by conventional combustion (below flammability limits of about 5–16%). The present study investigates the feasibility of capturing methane emissions from a compressor station. Computer modelling of the flow patterns of lean methane emissions inside the building is used to show the influence of doors, vents and leak location. Simulations show that for a typical building most fugitive methane exits through the ridge vent provided that the main doors remain closed. When the extraction rate through the ridge vent is controlled, the methane concentration is at acceptable levels for destruction in a catalytic flow reverse reactor, that is, in the range of 0.1–1% by volume.

Keywords: Fugitives; Greenhouse gas; Methane; Modelling

1. Introduction

Under the terms of the Kyoto Protocol, the governments of many countries, including Canada, have committed to reducing greenhouse gas (GHG) emissions. For example, Canada has committed to reduce to 6% below the 1990 emission level. A significant fraction of GHG originates from the use of energy, primarily because fossil fuels (coal, oil and natural gas) currently satisfy most of the global energy demands. Of the fossil fuels, natural gas has the lowest emissions of GHG per unit of energy, and there is much interest in switching from oil and coal to gas. However, while natural gas is significantly cleaner than other fossil fuel (combustion GHG emission from natural gas per unit energy produced is 25% and 40% less than oil and coal, respectively), non-combustion GHG emission (fugitive emissions) occurs during the process of extraction, production, processing, transmission, storage and distribution.

Among the primary GHGs of carbon dioxide, methane and nitrogen oxides (N_2O), the main contribution to global warming is made by CO_2 (about 64%), with the next largest contribution made by methane (about 19%) (Moore et al., 1998). GHG emissions are reported in terms of equivalent carbon dioxide emissions on a mass basis, calculated based on a warming potential for a 100-year lifecycle. Using this method, methane has a global warming potential 23 times that of CO_2, that is, 1 tonne of methane is equivalent to 23 tonnes of carbon dioxide. The combustion of methane thus offers the possibility of a net reduction in GHG potential of 88%. There are additional motivations for addressing methane. The atmospheric concentration of methane has been increasing at about 0.6% per year (Steele et al., 1992), and has more than doubled over the last two centuries (Intergovernmental Panel on Climate Change (IPCC), 1995). In contrast, carbon dioxide atmospheric concentration is increasing at about 0.4% per year. Reduction in methane emissions will

*Corresponding author. Tel.: +1 780 492 3571; fax: +1 780 492 2881.
E-mail address: bob.hayes@ualberta.ca (R. Litto).

0301-4797/$ - see front matter © 2006 Elsevier Ltd. All rights reserved.
doi:10.1016/j.jenvman.2006.06.007

Nomenclature

C_p	constant pressure heat capacity
$D_{i,m}$	diffusion coefficient of species i
$\tilde{F}$	other forces
$\tilde{g}$	acceleration due to gravity
h	enthalpy
h	heat transfer coefficient
I	unit tensor
$\tilde{J}_i$	diffusion flux of species i
k	thermal conductivity
k	turbulent kinetic energy
L	length from nearest wall
p	pressure
Pr_t	turbulent Prandtl number
Pr_{eff}	effective Prandtl number
q_t	turbulent heat flux
S_i	source term in species equation
S_h	source term in energy equation
Sc_i	Schmidt number of species i
T	temperature
$\tilde{u}$	mean velocity
u'	fluctuating velocity
v	magnitude of the local velocity
Δx_j	grid spacing adjacent to the wall
Y_i	mass fraction of species i

Greek letters

ρ	fluid density
$\tilde{\tilde{\tau}}$	shear stress tensor
μ	viscosity
μ_t	turbulent viscosity
μ_{eff}	effective viscosity

produce substantial benefits in the short term. Methane has a shorter atmospheric lifetime than other GHGs: methane lasts around 12 years in the atmosphere, whereas carbon dioxide lasts about 120 years (IPCC , 1992). Owing to methane's high effectiveness and short atmospheric lifetime, stabilization of methane emissions will have an immediate impact on mitigating potential climate change. A key challenge in the reduction of GHG is the mitigation of adverse economic impacts. Because methane is a source of energy as well as GHG, its emissions reduction strategies have the potential to be low cost, or even profitable. Fugitive methane reduction has the potential to produce immediate results with minimal adverse economic effects.

Although a variety of data have been published on methane emissions, such data should be treated with caution, and taken as general estimates only, because most of the data rely on many assumptions, and more reliable data will only emerge as additional emission audits are undertaken. Keeping this fact in mind, it is estimated that the main contributors to global methane emissions are agriculture (44%), landfills and biomass burning (22%), coal (12%) and the oil and gas industry (15%) (Moore et al., 1998). The 15% of emissions from the oil and gas industry equals about 47 Mt/yr (1081 Mt/yr of CO_2 equivalent), using 1990/92 data (Moore et al., 1998). Overall, it has been estimated that fugitive methane emissions account for about 50% of the GHG emissions of the Canadian conventional oil and gas sector. Estimates for the year 2000 by Environment Canada estimate total GHG emissions at 726 Mt of CO_2 equivalent, of which about 5.2% are fugitive methane emissions from the oil and gas sector (1.8 Mt of fugitive methane annually). Canada is responsible for about 2% of the global GHG emissions. There is a certain degree of inconsistency in the data, as noted, and it is probable that methane emissions are significantly underestimated.

In the oil and gas sector, methane emission occurs through leakage and venting of gases during normal operations, maintenance and system upset. Here, we use the term venting to describe streams that can be isolated as concentrated streams, whereas the term leakage refers to streams that, although initially concentrated, quickly become diluted with air and are thus at very low methane concentration. Frequently, the term "fugitive emissions" is used to refer to low concentration or lean streams. Typically, concentrated streams are easier to address, whilst leakage or fugitive streams tend to suffer more variability in flow rate and concentration, and are more difficult to deal with. Additionally, a problem in mitigating fugitives is to capture the methane so that it can be directed to a destruction source.

Sources of methane emissions in the natural gas sector include leaks in natural gas pipelines and compressor stations. Leakage occurs throughout the chain of activities, resulting from leaky seals, valves, pipe joints, compressor, etc. These emissions are expected to increase with increasing natural gas consumption, although at a lower rate than the rate of growth in the overall market. Improved management and maintenance, plus advances in technology, can potentially reduce the leakage and venting of methane from all parts of the operation.

For the reasons cited in the foregoing, the significance of promoting strategies to reduce the amount of methane discharged into the atmosphere is apparent. The purpose of this paper is to investigate the feasibility of capturing fugitive methane emissions that occur inside natural gas compressor buildings. Because natural gas compressor stations are a major source of fugitive methane emission, they can provide a convenient starting point for reduction efforts. Further, because the leak sources are enclosed, there is a better chance of implementing low-cost capture methods. In this paper, we report on the use of

computational fluid dynamics as a tool to investigate velocity, temperature and concentration distributions inside typical compressor buildings, and the efficacy of capturing these emissions for subsequent destruction.

2. Mitigation of methane emissions

A useful summary of classical mitigation options for methane is provided by the IEA (IEA GHG, 1999). For some specific solutions for the oil and gas sector, the paper by Hayes (2004) is also recommended. Restricting our mitigation options to combustion, there are two possibilities. Conventional (homogeneous) combustion is the most common type used, and often consists of a flare. Flares can be used for concentrated streams and for large volumes. The drawback of flares is that they are unpopular with the general public, and require the use of a support fuel if the heat content of the emission stream is not sufficiently high. Although the flame can be hidden from view in other types of thermal reactors, the constraint of the flammability limits remains. Methane emissions (especially fugitives) often consist of a low concentration mixture of methane and air that cannot be destroyed by conventional combustion, because their composition is outside the flammability limits (about 5–16% by volume for methane in air). Furthermore, many of these streams have variable composition and flow rate. These variations can occur over time scales varying from hours to days or months. For many streams catalytic combustion is a viable option, in which a suitable catalytic reactor is used to destroy the hydrocarbons. Catalytic combustion is a flameless combustion process that can be used to oxidize emissions that cannot sustain a conventional flame. Furthermore, catalytic combustion occurs at temperatures lower than conventional combustion processes and thus produces fewer harmful by-products. The combustion unit is usually smaller than a conventional firebox and can be located in areas where conventional, fired units would not be allowed (Hayes and Kolaczkowski, 1997).

Dilute methane streams from a compressor station are available at low temperatures. To achieve auto-thermal reactor operation in this case, a reactor requires significant feed pre-heating. To avoid feed pre-heating, a catalytic reverse flow reactor (CFRR) can be used. With reverse flow, the feed is periodically switched between the two ends of the reactor using control valves (Matros and Bunimovich, 1996). For an exothermic reaction, the CFRR exhibits a heat trap effect, which can be used to maintain an enhanced reactor temperature compared to a single-direction flow mode. The use of CFRR for the catalytic combustion of lean methane mixtures at ambient temperatures has been shown in several recent papers (Liu et al., 2000, 2001a–c; Aubé and Sapoundjiev, 2000; Salomons et al., 2003, 2004; Kushwaha et al., 2004, 2005). Specifically, the reactors reported on by Aubé and Sapoundjiev (2000), Salomons et al. (2003, 2004) and Kushwaha et al. (2004, 2005) were developed for the catalytic destruction of streams containing 0.1–1% v/v methane in air originating from underground coal mine ventilation air. The units can be scaled to the flow rate; one pilot unit reported on, for example, was 200 mm in diameter and could process of the order of 100 kg/h of gas (Salomons et al., 2003, 2004). We therefore have as a target for a building effluent stream, which is a mixture of methane and air to be in this concentration range.

3. Natural gas compressor stations

Natural gas is commonly transported to market through a pipeline network. When the gas flows through the pipelines, it loses pressure owing to friction, and the gas is periodically recompressed in compressor stations, located at distances of 100–150 km apart. These compressor stations typically contain between one and 15 compressors. The common types of compressors used are large slow-speed reciprocating compressors driven by natural gas internal combustion (IC) engines, or centrifugal compressors powered by natural gas-fuelled turbines.

There are three main sources of methane emissions in compressor stations. The first is emissions of methane resulting from incomplete combustion in the engine. The second results from instrument venting, whilst the third source is leaks in valves, flanges and other equipment inside the building. As noted, our focus in this work is the emissions in the building; however, for completeness we briefly describe the other two sources.

As noted, either turbines or natural gas IC engines are used to drive the compressors. While the emissions from gas turbines are fairly low, the IC engine emissions are significantly higher. These engines are operated in either lean burn (excess oxygen) or with a stoichiometric air/fuel ratio. The lean burn system produces less NO_X (by up to a factor of 10) and has better fuel economy than stoichiometric engines. Unfortunately, owing to a lower combustion temperature, the amount of methane in the exhaust gas of a lean burn engine is up to four times higher than for the stoichiometric version. From an economic perspective, the lean burn system is superior, and most units run in this mode. From an environmental perspective, the lean burn engine offers the advantage of low NO_X; however, normal lean burn operation may not yield sufficiently low NO_X values to meet some regulations, and thus some operators use stoichiometric operation in certain locations (e.g., California). Although the base NO_X emissions are high from a stoichiometric engine, the end of tailpipe emissions can be reduced to acceptable limits, and below that of lean burn operation, through the use of a three-way catalytic converter (TWC), like those used on automobiles for the past two decades.

If the NO_X is within acceptable limits with lean burn operation, catalytic converters are not usually used, and the emissions of methane are relatively high. A typical 115-l displacement natural gas lean burn engine running at 1200 rpm produces about 61 tonnes per year of methane

(1400 tonnes of CO_2 equivalent), which increases as the engines age.

The second emission source is instrument vents, which result from the use of natural gas as the supply medium for the pneumatic instruments used to control, for example, temperature and pressure. Pneumatic devices are often powered by natural gas because the high-pressure gas is readily available. These devices, however, bleed natural gas into the atmosphere during normal operation. This gas may be collected as a concentrated stream and vented outside the building.

The third source of methane emissions in compressor stations is leaking equipment. This source tends to be more prominent in older sites that are used to compress sweet gas. Because of the danger from sour gas (gas containing H_2S) leaks, stations that compress sour gas are much more tightly monitored and controlled than those pumping sweet gas. Methane losses through the compressor seal can range up to the tens of tonnes per year, and a single leaking valve can yield up to 1000 tonnes a year. Although the methane from leaks is of high concentration at the leak source, it quickly becomes diluted as it moves into the building and mixes with air, although in some cases the seal leaks may be collected and vented externally. The focus of this investigation was to understand the flow patterns and distribution of these leaks.

To illustrate the magnitude of the emissions problem, numbers from a typical site are given. These data were provided by Clearstone Engineering, Calgary, Alta. The site in question was a compressor station containing five compressors (four at 1650 hp and one at 1450 hp), a glycol dehydrator and two electric power generators. Natural gas was used to operate the instruments. Overall, 68% of the GHG emissions result from the fuel combustion in the engines, and the rest was mostly methane. Methane emissions from the building were about 930 tonnes a year, and a further 400 (estimated) tonnes per year resulting from incomplete combustion in the engines. The breakdown of the 930 tonnes was 49% from instrument venting, 36% from the produced water tank vent, 7% from fugitives, 7% from the glycol dehydrator and 1% from non-leaking sources. The economic value of this methane at $5 a GJ is about $500,000 a year.

4. Modelling methane fugitive flow

4.1. Methodology

The focus of this work was to develop an understanding of the flow pattern of fugitive methane emissions in a typical compressor building, and to show how methane leaking inside the structure can be captured. To explore different scenarios, we used computer modelling to simulate the flow of the methane in the building. This modelling was achieved by solving the appropriate partial differential equations that govern the conservation of momentum, mass and energy (see Section 4.4). The numerical solution of the equations was effected using a finite volume technique. We used Airpak V.2.1, which is a computational design tool for ventilation systems that are required to deliver indoor air quality, thermal comfort, health and safety, air conditioning and/or contamination control. Airpak uses the Fluent solver engine for concentration, energy and fluid flow calculations. The tool provides complete mesh flexibility, and allows the solution of flow in complex geometries using unstructured meshes (Fluent Inc., 2002). The solution domain was defined by the confining walls of the building. The engine, compressor, dehydrator and other equipment were modelled as simpler rectilinear or cylindrical shapes. The engine, compressor, dehydrator and exhaust pipe were treated as heat sources, and were the only sources of heat in the building. Steady-state simulations were performed.

4.2. Description of building models

Two buildings were modelled in this work. Both buildings were based on existing natural gas compressor stations located in the Province of Alberta, Canada. A typical expected range of emission rates was used, based on information from several sites. The first (small) building model contained a single engine and compressor combination. The building is 12.7 m long, 7.3 m wide and 6.5 m high (see Fig. 1). There are three louvers provided for ventilation, two doors on the north side (a large roll-up door, measuring 2.55 m wide by 4.37 m high and a smaller

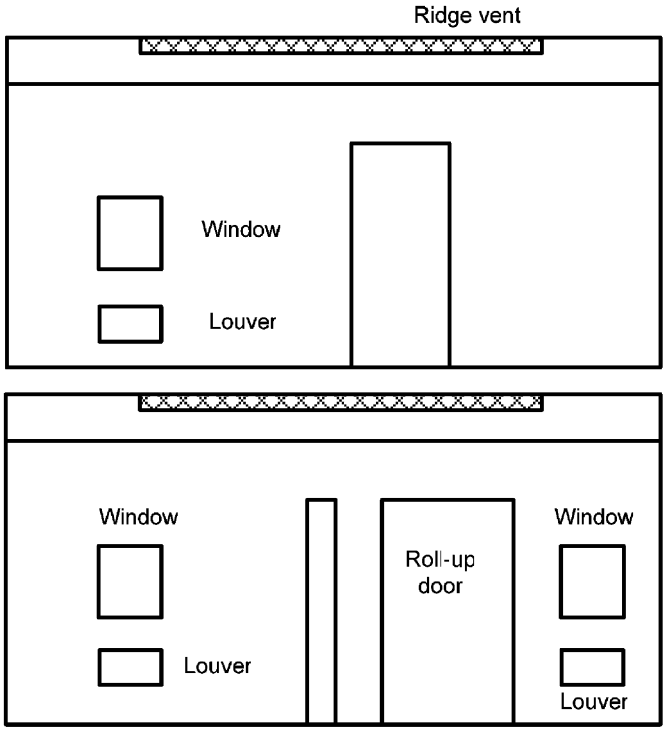

Fig. 1. Two side views of the building used as a model in this work. The top view is the south face with a single large door; the bottom view is the north face with the large roll-up door and a smaller door.

door measuring 1 m wide by 4.37 m high) and double doors on the south side measuring 1.91 m wide by 4.37 m high (see Fig. 1). Three windows are present, but these are usually closed. The smaller north door is also usually closed. The larger doors are often opened in the summer to provide additional ventilation, and are closed in the winter. A ridge vent along the top of the roof is used to assist extraction of building air. Fans are present to assist in ventilation, but are typically only used when large unexpected leaks occur. The compressor is powered by a Waukesha Model L5108 GSI, 12-cylinder, 84-l, turbo-charged, intercooled 1050 HP natural gas engine. Estimated methane emissions from this engine are 61 tonnes a year, based on data provided by Enerflex Systems Ltd., Edmonton, Alta.

The second building modelled contained 13 compressors. It is 77 m long, 9.9 m wide and 6.8 m high (see Fig. 2). For ventilation, it has 12 louvers on the upper part of the eastern wall. There are two large sliding doors, one each on the north and south ends, measuring 3.7 m wide by 3.1 m high, and seven exterior doors (measuring 1.0 m wide by 2.2 m high) each on the west and east sides. Also, there are seven emergency doors on the west side, but these are usually closed. A 0.5-m ridge vent along the top of the roof is used to assist extraction of building air. Fans are present to assist in ventilation, but again are typically only used when large unexpected leaks occur. In typical operation, eight out of 13 compressors are running with the others being used as backup. These compressors are driven by Waukesha 7042 GSI natural gas engines.

4.3. Modes of operation

The use of the stack effect, which utilizes the buoyancy principle, is the most common strategy in ventilation operation. The strategy uses the density difference between warm air inside the building and the cooler air outside. In this mode of operation, building outflow occurs through the ridge vent located at the apex of the roof. One of the key parameters, especially when retrofitting a building to mitigate emission, is to minimize the effect on operation by the implementation of mitigation technology. Therefore, we assume that collection of methane emissions will occur through the ridge vent. In the following sections, we begin by illustrating the flow patterns that are expected in existing situations, that is, we model simple natural flow with a free boundary at the ridge vent (“free flow” mode). In the second part, we impose a forced extraction rate at the ridge vent, which is equivalent to installing an extractor that operates at a specified flow rate. The effect of parameters on the capture efficiency and methane concentration in the effluent stream were investigated. The parameters are operating modes of building ventilation openings (doors, louvers, etc.), ambient conditions, ridge vent size and leak rate.

4.4. Model equations

The modelling of the building flow requires the solution of the governing conservation equations. These include turbulent momentum, mass and energy balance equations that include the effects of mixed convection. Generally, turbulence flows are predicted by three major approaches. Of these, direct numerical simulation (DNS) and large eddy simulation (LES) are too computationally costly, and therefore the Reynolds-averaged Navier–Stokes equations (RANS) were used. Averaging the Navier–Stokes equation to obtain the RANS equation introduces closure problems. RANS models come in a wide variety of forms. Each closes the system in some way, with the more complex models representing more of the underlying turbulence physics. The steady-state RANS equations take the following form.

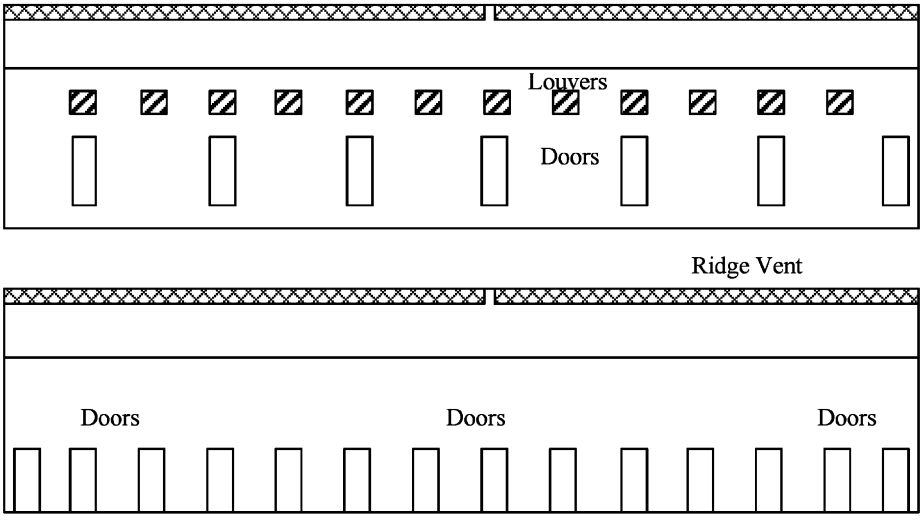

Fig. 2. Two side views of the large compressor building used as a model in this work. The top view is the east elevation with seven exterior doors; the bottom view is the west elevation with the seven exterior doors and seven emergency doors. The big sliding doors are on the south and north sides of the building, and are not shown in the drawing.

The continuity equation is

$$\nabla \cdot (\rho \tilde{u}) = 0. \tag{1}$$

The momentum transport equation:

$$\nabla \cdot (\tilde{u}\tilde{u}) = -\nabla p + \nabla \cdot \tilde{\tilde{\tau}} + \rho \tilde{g} + \tilde{F} - \nabla \cdot \left(\rho \overline{u'u'}\right). \tag{2}$$

Species balance:

$$\nabla \cdot (\rho \tilde{u} Y_i) = -\nabla \cdot \tilde{J}_i - \nabla\left(\rho \overline{Y_i u'}\right) + S_i, \tag{3}$$

where

$$\tilde{J}_i = -\rho\left(D_{i,m} + \frac{\mu_t}{\mathrm{Sc}_t}\right)\nabla Y_i. \tag{4}$$

Energy equation:

$$\nabla \cdot (\rho h \tilde{u}) = \nabla \cdot (k \nabla T) - \nabla\left(\rho C_{\mathrm{P}} \overline{Tu'}\right) + S_{\mathrm{h}}. \tag{5}$$

The additional term on these Reynolds-averaged transport equations accounts for the turbulence. Many RANS models assume a constitutive algebraic relationship between the Reynolds stress tensor and the mean flow gradients. The most common relationship is the eddy (or turbulent) viscosity model based on the Boussinesq assumption that the turbulent stress tensor can be expressed in terms of the mean rate of strain in the same way as the viscous stress for Newtonian isotropic fluids, except that the coefficient of molecular viscosity is replaced by eddy viscosity. The same principle applies to other constitutive relations for the flux of species and heat. The equations are

Turbulent stress:

$$\rho \overline{u'u'} = -\tilde{\tilde{\tau}}_{\mathrm{t}} = \tfrac{2}{3}kI - \mu_{\mathrm{t}}\left(\nabla \tilde{u} + \nabla \tilde{u}^{\mathrm{T}}\right). \tag{6}$$

Turbulent mass flux of species i:

$$\tilde{J}_{\mathrm{t}i} = \rho \overline{Y_i u'} = -\left(\frac{\mu_{\mathrm{t}}}{\mathrm{Sc}_{\mathrm{t}}}\right)\nabla Y_i. \tag{7}$$

Turbulent heat flux:

$$q_{\mathrm{t}} = \rho C_{\mathrm{P}} \overline{Tu'} = -\left(\frac{C_{\mathrm{P}}\mu_{\mathrm{t}}}{Pr_{\mathrm{t}}}\right)\nabla T. \tag{8}$$

Classic eddy viscosity models include mixing length models such as the zero-equation, one-equation and two-equation eddy viscosity models. The two-equation model, often referred to as the standard k–ε model, is the most widely used turbulence model in engineering practice. There are several variations of the $k-\varepsilon$ model. Many studies have used the k–ε model for indoor airflow analysis (for example, Awbi, 1989). To decrease computational time, Chen and Xu (1998) developed a zero-equation model specifically for modelling building enclosure airflows and heat transfer. This model uses an algebraic equation to calculate the local eddy viscosity instead of the differential equation for k–ε models. Chen and Xu (1998) tested this model on four airflow types: displacement ventilation, natural ventilation, forced convection and mixed convection. They found good agreement between the new zero-equation model predictions and the experimental data, and, in some cases the zero-equation models outperformed the $k-\varepsilon$ model. Srebric et al. (1999) provided further validation of this approach by comparing the predictive ability of the zero-equation models to experimental data for three additional cases of airflow in the enclosure. These include natural convection with infiltration, forced convection and mixed convection with displacement ventilation. They found good agreement between the computed and measured air velocity and temperature profiles.

The four eddy viscosity models used in Airpak V.2.1 are the mixing–length zero-equation turbulence model, the indoor zero-equation turbulence model, the standard and the renormalization group (RNG) $k-\varepsilon$ models. Preliminary investigations were performed using each of these turbulence models. The $k-\varepsilon$ models showed stability problems, whilst the indoor zero-equation model proved to be very stable. Chen and Xu (1998) recommends that the $k-\varepsilon$ model should be used for fully developed turbulence flows. The Reynolds number of the flow in this work is about 4200,which indicates that the flow is in transition turbulence. The Airpak manual suggests that the $k-\varepsilon$ model should be used for flow with very high Reynolds number. Based on these arguments and the preliminary investigations, the indoor zero-equation model was chosen for this work. In this model, the eddy viscosity is calculated by the relation proposed by Chen and Xu (1998), where L is the distance to the nearest wall and v is the magnitude of the local velocity:

$$\mu_{\mathrm{t}} = 0.03874 \rho v L. \tag{9}$$

The indoor zero-equation turbulence models can be used in natural, forced and mixed convection as well as displacement ventilation. In our work, we used the Boussinesq approximation to account for the density-driven flow, along with the ideal gas assumption.

The boundary conditions used were as follows. At the solid surfaces a zero-slip condition was employed for the velocity. The heat transfer at the boundary surface is determined by computing a convective heat transfer coefficient using the following relationship:

$$h = \frac{\mu_{\mathrm{eff}} C_{\mathrm{P}}}{Pr_{\mathrm{eff}} \Delta x_j} \quad \text{and} \quad \mu_{\mathrm{eff}} = \mu + \mu_{\mathrm{t}}. \tag{10}$$

For the equipment inside the building, the surface temperatures were fixed for those bodies generating heat, which include the engine, compressor and exhaust pipe. These units provide the heat sources inside the building. The mass flux at the walls was set to zero. For the openings, in free flow mode a free boundary condition was used. For forced extraction on the ridge vent, a mass flow rate was specified. When the external wind effects were investigated, velocities were imposed on the openings. We used the algebraic multigrid method, with first-order upwinding and under-relaxation. For the small building about 300 000 hexahedral mesh elements were used, and for the large one about 3 500 000 hexahedral elements were used.

5. Results and discussion

5.1. Free flow in small building

The first results presented were obtained with quiescent air surrounding the small building at an ambient temperature of 293 K. For these simulations, the free flow mode was used. Four combinations of operating mode were explored, denoted as follows: Option 1, all doors closed, Option 2, only north side roll-up door open; Option 3, north roll-up and south door open; and Option 4, all the doors were open. Two ridge vent sizes were used, with areas of 5 and 1 m^2. Three fugitive leak sources were imposed near the engine, with a total leak rate of either 2.7 or 270 kg/h. The principal variables of interest are the fraction of leaking methane flowing through the ridge vent, the average methane concentration in this stream, the temperature of the stream and the total mass flow of the stream. Table 1 shows a summary of the results obtained for the above conditions.

Several trends are evident from the data, some of which are not surprising. If we consider that the methane flowing through the ridge vent can be captured, we see that the best capture rate is obtained when all the doors are closed. With the louvers located near the bottom of the building, and the temperature within the building higher than ambient, the stack effect naturally leads to a flow upwards. As the doors are progressively opened, more methane flows through these openings, giving a low capture rate. There is no meaningful difference between capture rates for the different vent sizes when the doors are closed; however, the larger vent is generally superior when the doors are opened. Concentration of methane in the ridge vent stream is generally too low for the CFRR when the leak rate is low, although it increases to an acceptable level for high emission rates. For these levels of emissions, however, it would likely be better to eliminate the leaks rather than simply to mitigate them by combustion. The temperature of the effluent stream is the highest when the doors are closed, which corresponds to the lowest mass flow rate. The temperature rise is fairly low in all cases. Note that under free flow mode the total exchange rate in the building corresponds to about 13 building changes per hour.

Table 2 summarizes the results obtained for the small compressor building with an imposed velocity of 2 m/s blowing from north to south. To impose a wind, we approximated the effect by imposing an additional input velocity on the open doors. This method is an approximation, but serves to illustrate the effect of additional airflow through the doors. In any case, the capture rate with the doors open remains low. The ambient temperature was 293 K and the leakage rate was 2.7 kg/h. There is little effect when the doors are closed. When the north door is open and the others closed, a slight increase in the capture rate is observed, whilst in other cases the capture decreases. The concentration is also below that required for the CFRR.

Fig. 3 shows the effect on the mass flow rate through the ridge vent as the temperature outside the building is lowered. These results were obtained with a leak rate of 2.7 kg/h with the doors closed. From the graph it can be observed that the mass flow rate decreases as the ambient temperature falls, and when the ambient temperature is below 0 °C the flow through the ridge vent is positive, which means the flow direction is into the building. This effect is related to the pressure differential between the inside and outside of the building, which in turn depends on the buoyancy effects generated by the temperature

Table 1
Summary of results obtained for the small compressor building with quiescent air at 293 K operated in free flow mode

Option	Leak rate, kg/h	Vent size, m^2	% Methane captured	Mole % methane	Mass flow rate, T/h	Temperature, K
1	2.7	5	97.4	0.037	10.4	309
2	2.7	5	88.0	0.014	24.5	302
3	2.7	5	82.8	0.013	24.8	302
4	2.7	5	65.3	0.010	24.9	302
1	270	5	96.3	0.43	10.5	306
2	270	5	78.9	0.14	25.0	301
3	270	5	70.0	0.13	25.1	301
4	270	5	64.8	0.11	27.5	300
1	2.7	1	99.7	0.061	6.4	309
2	2.7	1	36.1	0.023	6.4	306
3	2.7	1	32.4	0.021	6.2	306
4	2.7	1	29.4	0.019	6.1	306
1	270	1	98.1	0.67	6.8	305
2	270	1	36.5	0.25	7.0	304
3	270	1	13.5	0.093	7.0	300
4	270	1	22.3	0.17	6.5	301

Conditions at the ridge vent.

Table 2
Summary of results obtained for the small compressor building with an imposed velocity of 2 m/s blowing from north to south

Option	Vent size, m^2	% Methane captured	Mole % methane	Mass flow rate, T/h	Temperature, K
1	5	98.6	3.7	9.2	304
2	5	99.4	1.3	25.0	300
3	5	65.2	0.9	23.2	300
4	5	48.5	0.6	23.1	300
1	1	98.2	8.6	4.5	302
2	1	38.2	2.5	6.1	301
3	1	15.3	1.5	4.0	300
4	1	16.0	1.6	4.1	300

Ambient temperature of 293 K operated in free flow mode. The leakage rate was 2.7 kg/h. Conditions at the ridge vent.

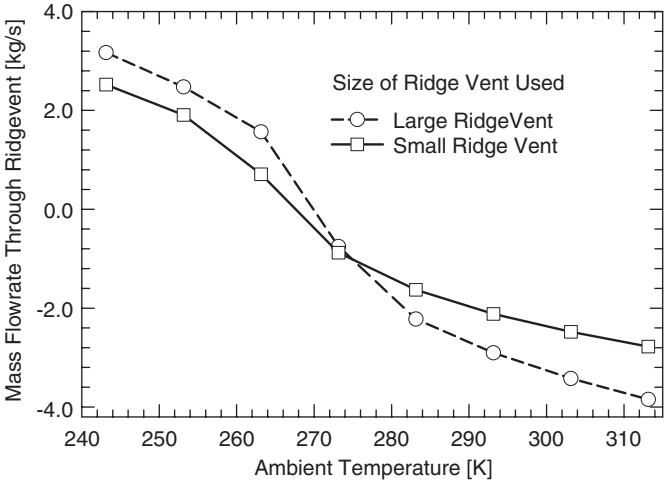

Fig. 3. Effect of external temperature on the mass flowrate through the ridge vent. A negative value indicates a flow out of the building.

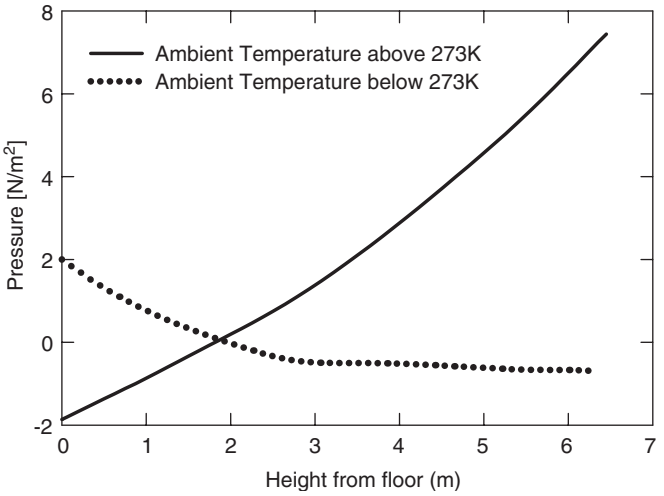

Fig. 4. Pressure profile in the middle of the building as a function of the external temperature. The pressure profile depends on the temperature.

inside. Fig. 4 shows the change in the pressure profile (difference between internal and external pressure) as the ambient temperature changes. At high ambient temperature, the external pressure gradient decreases faster than the internal pressure, thus forcing flow out through the ridge vent. As the temperature falls, the rate of change within the building also changes, until at low temperature the pressure at the top of the building is higher outside than inside. This pressure differential forces flow inwards through the ridge vent. Fig. 5 shows the effect on the circulation pattern as a function of the ambient temperature. The complexity of the flow pattern and the temperature effect is evident. The methane exits through the louvers and in this case, no methane can be captured at the ridge vent.

In the results discussed above the building was considered to have no obstacles on flow space above the engine, compressor, etc. Simulations were repeated with some additional piping added in the flow space, and the results are summarized in Table 3. The general trend is the same as observed before, although some variations were seen in methane capture and concentration.

5.2. Forced extraction in small building

Simulation of the free flow mode of operation gives a good insight into the nature of the flow patterns within a typical building. The general observation is that for a low leakage rate the concentration of methane at the ridge vent is too low for the CFRR. This low concentration is the result of the high mass flow rate that is induced by natural convection forces. The large flow rate implies that a large reactor would be required, which adds unnecessarily to the capital cost. Further, for low ambient temperature, the natural flow rate is through the vent into the building, that is, the methane emissions leave via the louvers, and not the ridge vent. Considering that some extraction device is required to direct the effluent into the reactor, we now examine the effect of controlling the exhaust gas flow rate through the ridge vent. We simulate this effect by imposing a constant mass flow rate at the vent.

Experiments on the controlled extraction mode of operation were performed using building operating Options 1 and 2 only, since these were the options that gave a promising result in the free flow experiments. Several extraction rates combined with different leak rates were

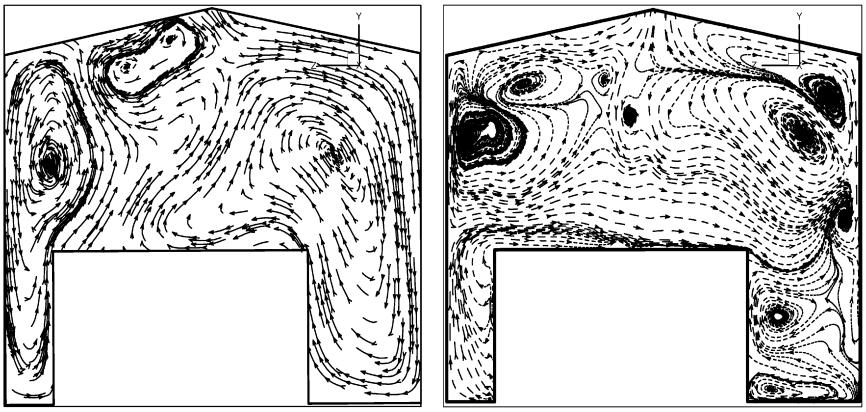

Fig. 5. Airflow pattern inside the building for (left) ambient temperature below 273 K and (right) ambient temperature is above 273 K.

Table 3
Summary of results obtained for the small compressor building with quiescent air at 293 K operated in free flow mode, with added piping in the building

Option	Leak rate, kg/h	Vent size, m^2	% Methane captured	Mole % methane
1	2.7	5	93.5	0.034
2	2.7	5	91.8	0.013
3	2.7	5	88.9	0.013
4	2.7	5	85.6	0.011
1	270	5	97.7	0.45
2	270	5	82.5	0.15
3	270	5	77.3	0.14
4	270	5	64.8	0.11
1	2.7	1	88.5	0.052
2	2.7	1	49.1	0.025
3	2.7	1	39.5	0.020
4	2.7	1	39.9	0.020
1	270	1	99.9	0.71
2	270	1	32.7	0.23
3	270	1	43.3	0.10
4	270	1	8.4	0.067

Conditions at the ridge vent.

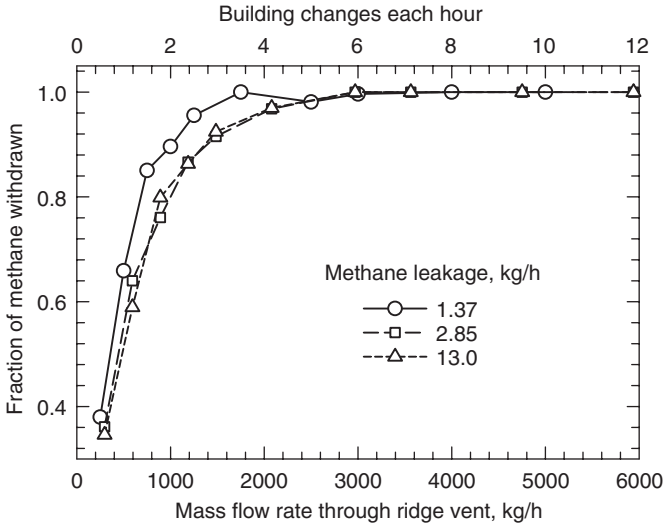

Fig. 6. Fraction of methane captured through ridge vent using forced extraction in the small building with the doors closed, at three leak rates. Above about four room changes an hour most of the methane is captured. The ambient temperature was 303 K.

used. Fig. 6 shows the effect of extraction rate on the fraction of methane recovered at three different leak rates with an ambient temperature of 303 K. The operating mode was Option 1, all doors closed. It is seen that the fractional recovery is essentially independent of the leak rate, and depends only on the extraction rate. Above about four building changes an hour essentially all of the leaking methane is captured. Fig. 7 shows how the concentration of the methane in the extracted stream varies with the extraction and leakage rates. In this case, it is clear that the methane concentration increases with leak rate, and decreases with extraction rate. These results follow intuitively from normal dilution rules. It is clear from this figure that controlling the extraction rate can give suitable feed for the CFRR (between 0.1% and 1% volume methane). Figs. 8 and 9 show the effect of extraction rate on the fraction of methane recovered and concentration of methane in the extracted stream, respectively, for operation with Option 2. It is clear that methane concentration and capture rate are greatly reduced by opening the large doors.

Figs. 10 and 11 show the velocity patterns in the building for Options 1 and 2, respectively. It is clearly seen that the buoyancy effect induces strong recirculation patterns, which are expected to cause efficient mixing of the methane, which leads to difficulty in capturing concentrated methane emissions. Strong upward flows are seen around the hot engine. The effect of ventilation openings (doors and louvers) on the fugitive methane capture can be observed by comparing the velocity patterns in Fig. 10, (Option 1) to those in Fig. 11 (Option 2). In Fig. 10, air enters only through the louvers, and the gas exits only through the ridge vent after being mixed in the building. In Fig. 11(b), it is seen that significant exchange of building and external air occurs through the open door. The cold air

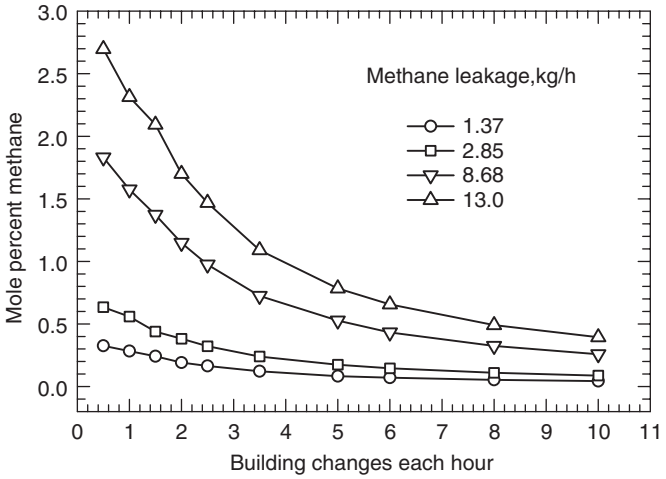

Fig. 7. Mole percentage of methane in the ridge vent effluent obtained using forced extraction from the small building with the doors closed. The ambient temperature was 303 K. The effect of extraction rate and leakage rate are shown.

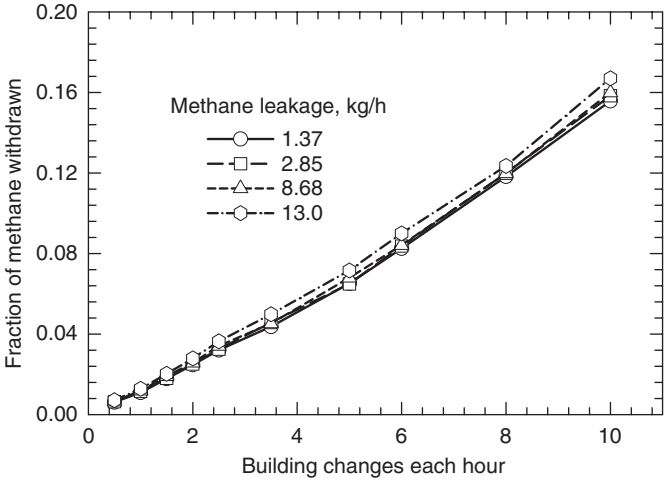

Fig. 8. Fraction of methane captured through ridge vent using forced extraction in the small building with the large roll-up doors opened. The ambient temperature was 303 K.

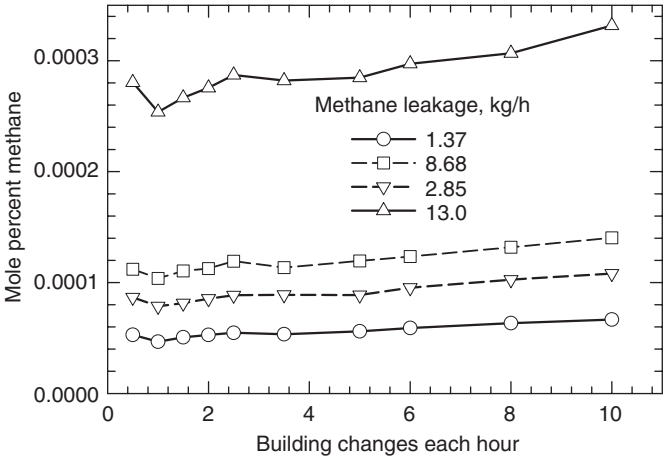

Fig. 9. Mole percentage of methane in the ridge vent effluent obtained using forced extraction from the small building with the large roll-up door opened. The ambient temperature was 303 K. The effect of extraction rate and leakage rate are shown.

flows into the building at the bottom of the opened door, mixes with the gases inside the building and then flows out the building at the top of the opened door. This makes the maximum capture of the fugitive methane impossible, and explains why earlier it was suggested that the best way to operate is with all doors closed. It is clear that opening the doors has a strong effect on the flow and recirculation patterns.

Methane mole fraction profiles in the building are shown in Figs. 12 and 13. Generally, speaking, the methane mole fraction at the bottom of the building is lower, and increases as one ascends to the top of the building. Fig. 12 shows that by closing the doors, the goal of raising the concentration of methane in the captured stream to meet the CFRR feed requirements can be achieved. Operating with Option 2, where the large roll-up door is open, not only increases the air dilution inside the building but also provides an escape route for the fugitive methane emitted in the building. Profiles of methane mole fraction shown in Fig. 13 suggest that with the doors open, the concentration of methane in the building will be very low and thus make it difficult to meet the CFRR feed quality requirements.

In the free flow mode, the flow rate through the ridge vent was affected by the ambient temperature. Thus, when operating with ambient temperature below 273 K, the net flow through the ridge vent was into the building. When imposing a flow at the vent, this reversal is obviously impossible. To test the effect of ambient temperature, simulations were performed with ambient temperature below 273 K, and no effect on the flow was observed. Typical results are shown in Figs. 14 and 15. The results are essentially the same as those observed with ambient temperature is above 273 K (see Figs. 6 and 7). Thus, ambient temperature has essentially no effect on the flow rate or concentration of effluent of the ridge vent effluent.

5.3. Free flow in large building

The simulation of large building was carried out with ambient temperature of 293 K. For the case of free flow mode, five building operating options were explored, denoted as follows: Option A, all doors are opened; Option B, only north and south side doors are closed; option C, north, south and east doors are closed; Option D, north, south and west doors are closed; and Option E, all doors are closed. In all options the louvers and ridge vents are used to ventilate the building unless stated otherwise. Two different cases were considered in regard to louvers location. In Case 1 the louvers were located at the top of the building (the current operating position) and in Case 2 the louvers were located at the bottom of the building, as in the small compressor building. In this latter

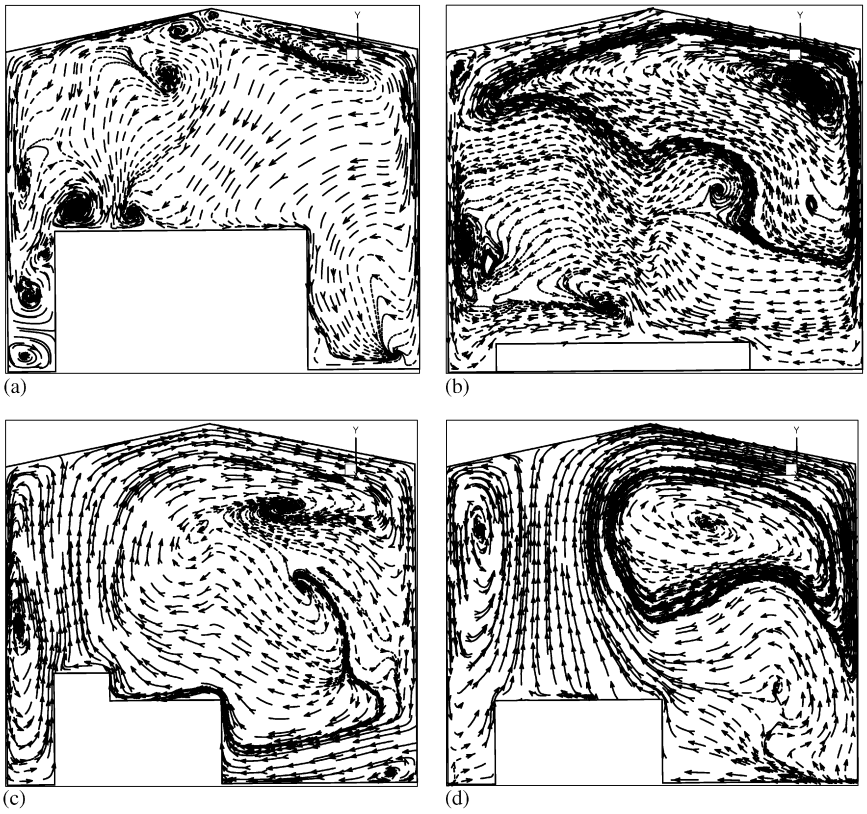

Fig. 10. Velocity vectors in the small compressor building operating with Option 1 with controlled extraction. The velocity vectors were taken (a) at the south side louvers position; (b) at the roll-up door position; (c) at the engine, turbo charger and exhaust pipe position, which is the hottest position in the building and near the north-east louver; (d) slightly further along the engine position. Plane of vectors is the building vertical cross section.

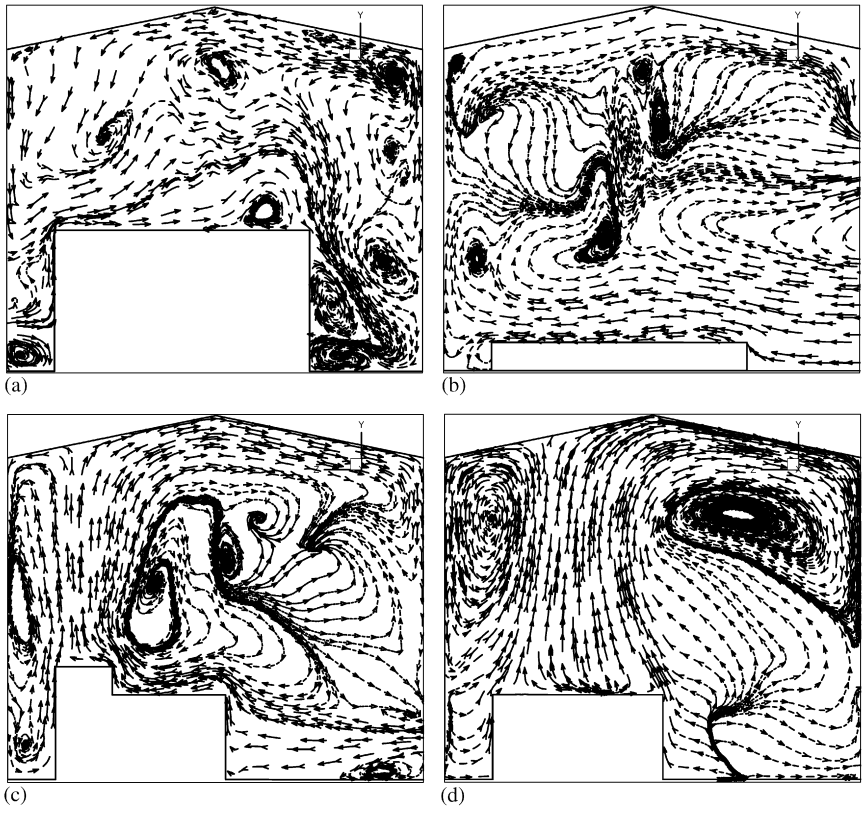

Fig. 11. Velocity vectors in the small compressor building operating with Option 2 under controlled extraction case. Building slices taken at same positions as in Fig. 8.

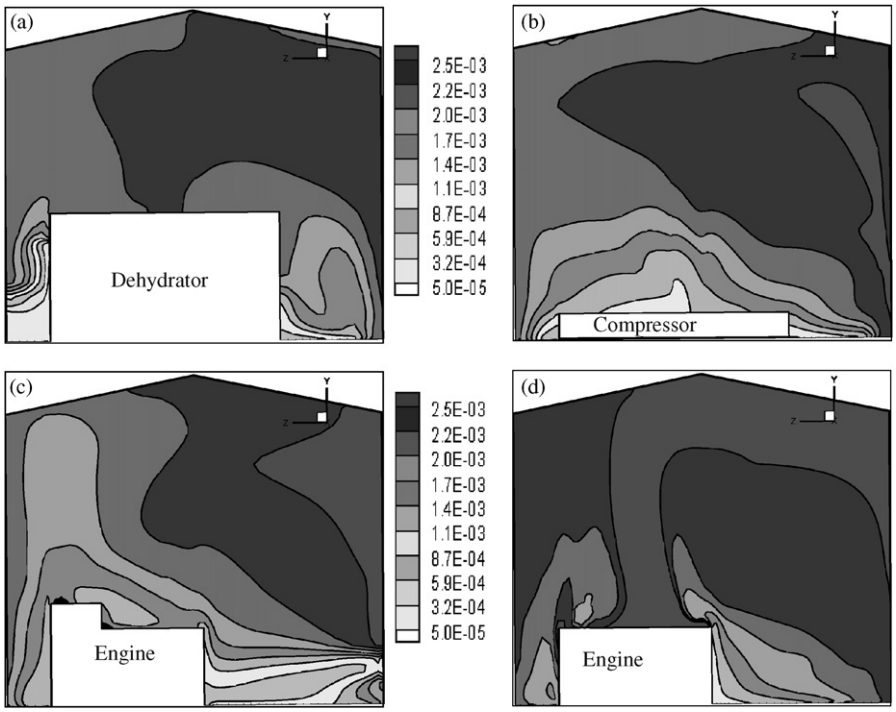

Fig. 12. Profile of methane mole fraction in the small compressor building operating with Option 1 under controlled extraction case. The mole fraction profiles were taken at (a) south side louvers position; (b) the roll-up door position; (c) engine, turbo charger and exhaust pipe position which is the hottest position in the building and also corresponds to the position of the north-east louver; and (d) the engine position.

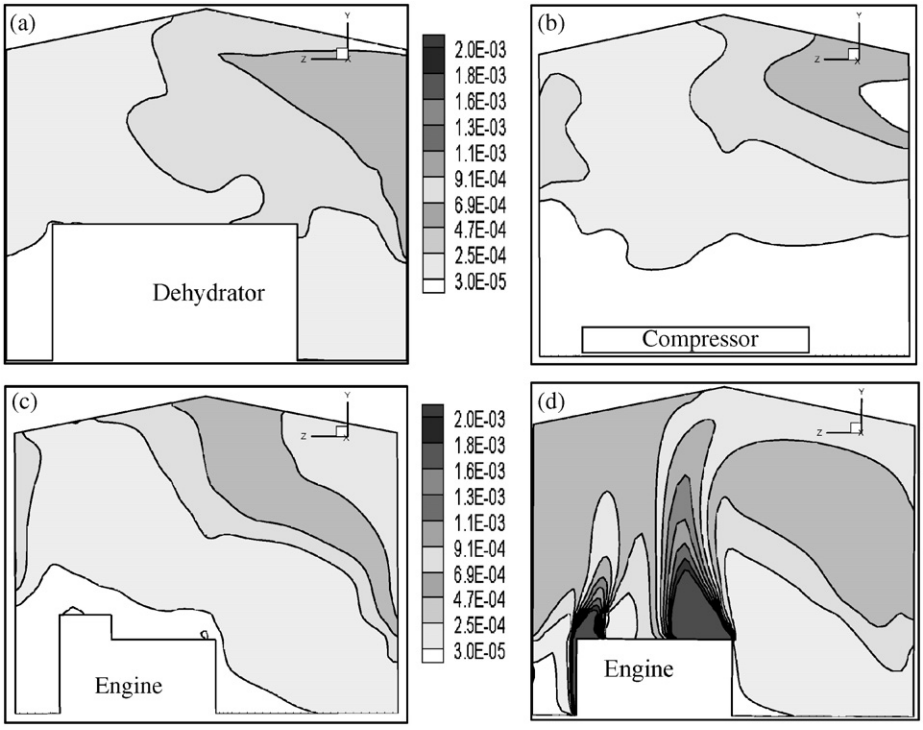

Fig. 13. Profile of methane mole fraction in the small compressor building operating with Option 2 under controlled extraction case. The mole fraction profiles were taken at the same locations as in Fig. 10.

case, the louvers were located between the doors shown in the figure. The fugitive leak sources were imposed and distributed around the building, with a total leakage rate of 278 kg/h. Table 4 shows a summary of the results obtained from the simulation carried out with the above conditions.

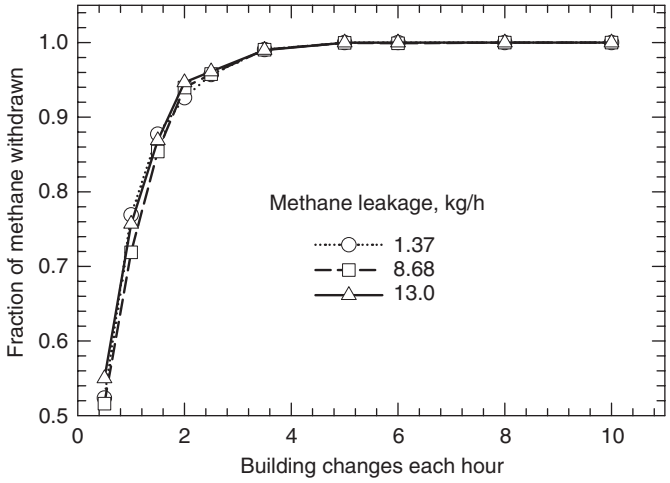

Fig. 14. Fraction of methane captured using forced extraction in the small building with the doors closed, at three leak rates. Above about four room changes most of the methane is captured. The ambient temperature is below 273 K.

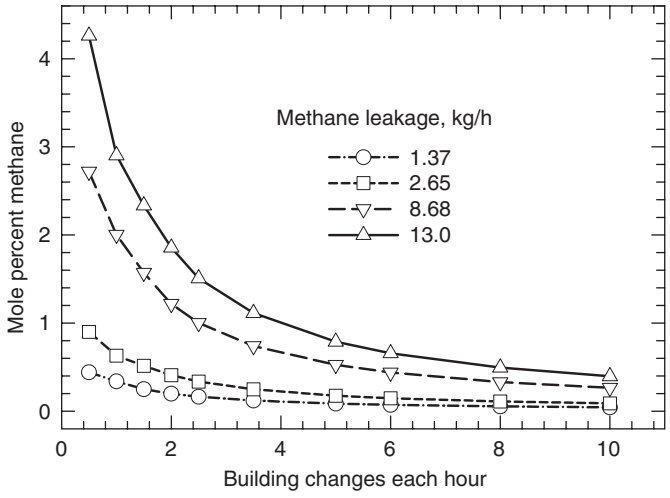

Fig. 15. Mole percentage of methane in the extracted stream versus extraction rate at different leak rates in the small building. The ambient temperature is below 273 K.

For the free flow case the trend is the same as observed in the small building. Opening the doors increases the flow rate through the ridge vent and reduces the concentration. As previously observed, the concentration through the ridge vent is below that required for the CFRR.

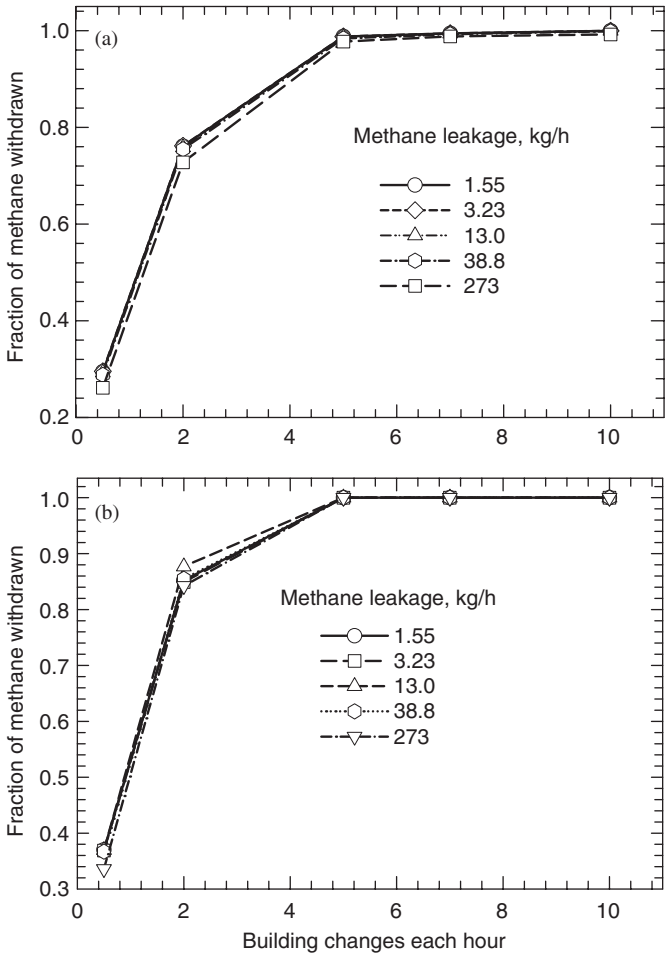

Fig. 16. Fraction of methane captured using forced extraction in the large compressor building with the doors closed. Above about five room changes most of the methane is captured. Louvers on the east wall at (a) the top and (b) the bottom.

Table 4
Summary of results obtained for the large compressor building with quiescent air at 293 K operated in free flow mode (with louvers on the current side of the wall), total leakage rate was 278 kg/h and the area of the ridge vent was 38.4 m^2

Option	Louvers position	% Methane captured	Mole % methane	Mass flow rate, T/h	Temperature, K
A	Top	93.2	0.204	235	294
B	Top	100.0	0.231	215	299
C	Top	98.1	0.265	183	301
D	Top	94.1	0.269	171	301
E	Top	81.7	0.533	77	304
A	Bottom	91.5	0.210	218	292
B	Bottom	98.2	0.245	203	299
C	Bottom	100.0	0.300	171	301
D	Bottom	95.8	0.303	160	302
E	Bottom	68.2	0.602	57	305

Conditions at the ridge vent.

5.4. Forced extraction in large building

Experiments using the controlled extraction mode of operation were carried out using Cases 1 and 2, with Option E. Several extraction and leakage rates were used. Fig. 16 shows the effect of extraction rate on the fraction of methane recovered at different leak rates with the louvers located at the top and bottom of the east wall. It can be seen that the fractional recovery is essentially independent of the leak rate, and depends only on the extraction rate, as was observed in the small compressor building. The methane mole fraction in the ridge vent effluent is shown in Fig. 17 for both cases. These results suggest that the CFRR feed quality requirements can be achieved by controlling the extraction rate. Further, these figures suggest that the location of the louvers has only a small effect on methane recovery fraction and concentration. Although at low extraction rate the difference in performance due to louvers location can be observed, in practice it is not recommended to operate the building at such low extraction rates.

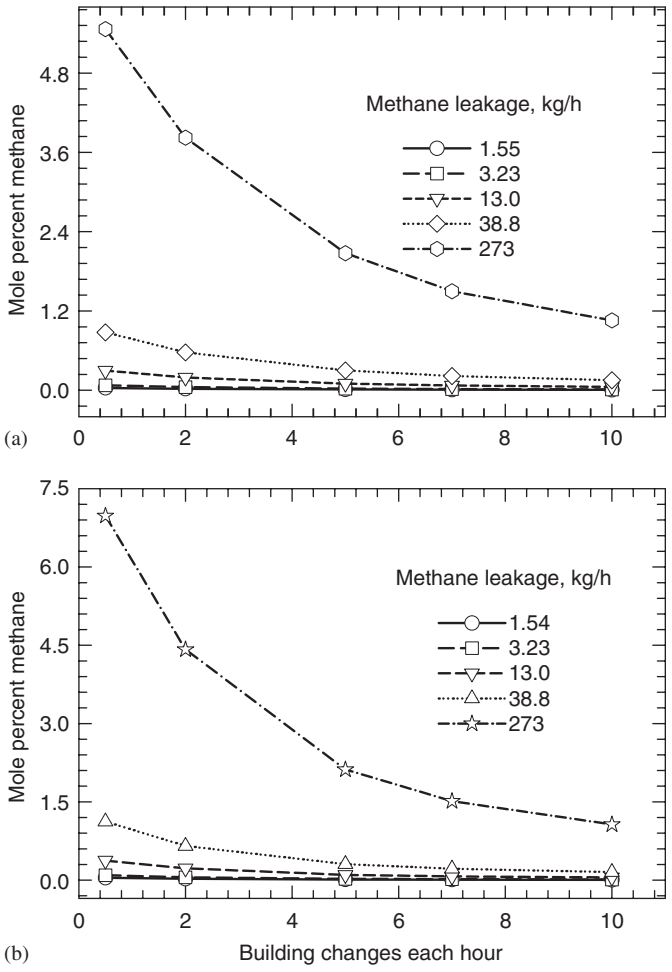

Fig. 17. Mole percentage of methane in the extracted stream versus extraction rate at different leak rate. Louvers located on the east wall at (a) the top and (b) the bottom.

The velocity vector and methane mole profile for the large compressor building generally follow similar patterns to those observed in the small compressor building. The opening or closing of the doors, and the location of the louvers, have been shown to be the main factors in achieving a good capture and methane concentration in the effluent stream.

6. Conclusions

Fugitive methane emissions in the oil and gas sector are a major contributor to GHG emissions. At the same time, they are potentially much easier to reduce or eliminate than gases such as carbon dioxide, which is very expensive to capture and sequester using current technology. Fugitive emissions in natural gas compressor stations can potentially be collected using the building itself. Possibly the most important variable that affects the capture rate is the opening of the large doors. The large doors are often opened in the summer to keep the building cool. Using controlled extraction rates, typical emission rates can lead to an acceptable feed for a reverse flow catalytic reactor. This effluent can also be potentially combined with instrument vent streams, or the engine exhaust stream (which also contains significant methane and carbon monoxide), to increase the reduction of GHG emissions.

Acknowledgements

Financial support was provided by the Natural Sciences and Engineering Research Council of Canada (NSERC), Natural Resources Canada (NRCan) and the Alberta Energy Research Institute (AERI) via Course Grant 1472. CANMET Energy Technology Centre Varennes, BP Canada Energy Company, New Paradigm Engineering, Clearstone Engineering, TransCanada Pipelines Ltd. and Enerflex Systems Ltd. provided data and technical input.

References

Aubé, F., Sapoundjiev, H., 2000. Mathematical model and numerical simulations of catalytic flow reversal reactors for industrial applications. Computers and Chemical Engineering 24, 2623–2632.

Awbi, H.B., 1989. Application of computational fluid dynamics in room ventilation. Building and Environment 24, 73–84.

Chen, Q., Xu, W., 1998. A zero equation turbulence model for indoor airflow simulation. Energy and Buildings 28, 137–144.

Fluent Inc., 2002. Airpak 2.1 User's Guide.

Hayes, R.E., 2004. Catalytic solutions for fugitive methane emissions in the oil and gas sector. Chemical Engineering Science 59 (16), 4073–4080.

Hayes, R.E., Kolaczkowski, S.T., 1997. Introduction to Catalytic Combustion. Gordon and Breach Science Publishers, Reading, UK.

IEA GHG, 1999. Technologies for the Abatement of Methane Emissions. IEAG/SR7,IEA R&D Greenhouse Gas Programme, Cheltenham, UK.

Intergovernmental Panel on Climate Change (IPCC), 1992. In: Houghton, J.T., Jenkins, G.J., Ephraums, J.J. (Eds.), Climate Change 1992: The Supplementary Report to the IPCC Scientific Assessment. Published for the Intergovernmental Panel on Climate Change, World

Meteorological Organization/United Nations Environment Program. Cambridge University Press, Cambridge.

Intergovernmental Panel on Climate Change (IPCC), 1995. In: Watson, R.T., Zinyowera, M.C., Moss, R.H., Dokken, D.J. (Eds.), Climate Change 1995, Impacts, Adaptations, and Mitigation of Climate Change: Scientific Technical Analysis, Contribution of Working Group II to the Second Assessment Report of the Intergovernmental Panel on Climate Change. Cambridge University Press, Cambridge, UK (1996).

Kushwaha, A., Hayes, R.E., Poirier, M., Sapoundjiev, H., 2004. Effect of reactor internal properties on the performance of a flow reversal catalytic reactor for methane combustion. Chemical Engineering Science 59 (16), 4081–4093.

Kushwaha, A., Hayes, R.E., Poirier, M., Sapoundjiev, H., 2005. Heat extraction from a flow reversal reactor in lean methane combustion. Chemical Engineering Research and Design, Transactions of the Institute of Chemical Engineers, Part A 83 (A2), 205–213.

Liu, B., Checkel, M.D., Hayes, R.E., Zheng, M., Mirosh, E.A., 2000. Transient simulation of a catalytic converter for a dual fuel engine. Canadian Journal of Chemical Engineering 78, 557–568.

Liu, B., Checkel, M.D., Hayes, R.E., Zheng, M., Mirosh, E.A., 2001a. Experimental and modelling study of variable cycle time for a reversing flow catalytic converter for natural gas/diesel dual fuel engines. SAE Transactions, Journal of Fuels and Lubricants 109 (4), 15.

Liu, B., Hayes, R.E., Checkel, M.D., Zheng, M., Mirosh, E., 2001b. Reversing flow catalytic converter for a natural gas/diesel dual fuel engine. Chemical Engineering Science 56, 2641–2658.

Liu, B., Checkel, M.D., Hayes, R.E., 2001c. Experimental study of a reverse flow catalytic converter for a dual fuel engine. Canadian Journal of Chemical Engineering 79, 491–506.

Matros, Y.S., Bunimovich, G.A., 1996. Reverse-flow operation in fixed bed catalytic reactors. Catalytic Reviews: Science and Engineering 38, 1–68.

Moore, S., Freund, P., Riemer, P., Smith, A., 1998. Abatement of methane emissions. IEA Greenhouse Gas R&D Programme, Cheltenham, ISBN:1-898373-16-7.

Salomons, S., Hayes, R.E., Poirier, M., Sapoundjiev, H., 2003. Flow reversal reactor for the catalytic combustion of lean methane mixtures. Catalysis Today 83, 59–69.

Salomons, S., Hayes, R.E., Poirier, M., Sapoundjiev, H., 2004. Modelling a reverse flow reactor for the catalytic combustion of fugitive methane emissions. Computers and Chemical Engineering 28 (9), 1599–1610.

Steele, L.P., Dlugokencky, E.J., Lang, P.M., Tans, P.P., Margin, R.C., Masarie, K.A., 1992. Slowing down of the global accumulation of atmospheric methane during the 1980s. Nature 358 (6384), 313–316.